J. Synchrotron Rad. (1995). **2**, 215–228

Evaluation of Charge-Injection Devices for Use in Laue Diffraction Imaging

Quentin S. Hanley, J. Bruce True and M. Bonner Denton*

Department of Chemistry, University of Arizona, Tucson, AZ 85721, USA

(*Received 21 March 1995; accepted 13 June 1995*)

Charge-injection devices (CIDs) are versatile detectors having a number of features which recommend them for use in the imaging of X-ray diffraction patterns. They have a flexible nondestructive readout allowing for analysis of image quality during data collection and rapid readout of selected portions of the device. CIDs have full-well capacities in the range of 10^6 charge carriers giving them a high dynamic range for both direct and indirect imaging of X-rays. CIDs have peak quantum efficiencies in the optical region over 50% allowing for their incorporation into indirect detection systems. Rapid random single-pixel address allows for their use as single X-ray photon counters with energy discrimination. Three types of position-sensitive detectors for X-rays have been developed using CIDs. Two CID formats, the CID 17PPRA (388 × 256) and the CID 38SG (512 × 512), were incorporated into systems performing indirect imaging, direct imaging and single X-ray photon counting with energy discrimination. Indirect images of the Laue diffraction patterns from tetraphenylphosphonium tetrachlorooxomolybdenum(V) and natural MoS_2 were collected using a phosphor sheet to convert X-rays into optical photons which were detected with the CID 38SG. Directly detected images of spots from the Laue diffraction pattern of MoS_2 were recorded with the CID 17PPRA. Single photon counting with energy discrimination is demonstrated with the CID 17PPRA using a reflection from the Laue diffraction pattern of MoS_2. Useful information could be obtained from a single pixel at read rates over 7 kHz. Complete energy-dispersive analysis suitable for determination of space groups from Laue diffraction is currently limited due to incomplete charge collection and/or split events.

Keywords: charge-injection devices; Laue diffraction; area detectors; X-ray detection.

1. Introduction

A number of detector systems are available for use in the detection of X-rays in crystallographic applications. These include: photographic film, scintillation detectors, image plates (Miyahara, Takahashi, Amemiya, Kamiya & Satow, 1986), multiwire detectors (Xuong, Freer, Hamlin, Nielson & Vernon, 1978), silicon intensified targets (SITs) (Arndt, 1990; Li, Phillips, Stanton & Kalata, 1992), charge-coupled devices (CCDs) (Phillips, Li, Stanton, Xie & O'Mara, 1993; Allinson, 1989) and a variety of image intensifiers. All of these systems are in current use and they vary widely in quantum efficiency, dynamic range and spatial resolution (Helliwell, 1992). Charge-injection device (CID) detection offers a unique readout architecture combining many of the capabilities of these detectors including direct and indirect imaging and single X-ray photon counting.

The goal of this research is to develop instrumentation for energy-resolved area detection for use in Laue diffraction applications. Work toward this goal has led to an investigation of charge-injection devices. CIDs have the capacity to operate over a wide dynamic range in indirect imaging and to operate as single X-ray photon counters in direct detection. Laue diffraction has long offered the potential for being the fastest method for crystallographic structure determination and partial realization of this potential has been achieved (Coppens, 1992; Helliwell, 1992). Complete exploitation of the Laue experiment for crystallography requires that some form of energy-resolved instrumentation be developed to solve problems currently limiting its use in the routine analysis of crystal structures.

When the energy bandwidth of the incident 'white' beam in a Laue experiment is sufficiently wide, multiple orders of diffraction can be observed. This results in the overlapping orders problem (Helliwell, 1992), in which reflections appear at the same position in space but with energies consisting of integral sub-multiples of λ/n (*i.e.* harmonics). Depending on the energy bandwidth of the incident beam, the overlapping orders may obscure the systematic absences useful for space-group determination. The reflections produced from overlapping orders represent approximately 10–20% of all reflections (Cruickshank, Helliwell & Moffat, 1987) and are not routinely used in structure refinement. It would be desirable to allow these

* Author to whom correspondence should be addressed.

reflections to be used for both space-group determination and structure refinement. Although recent progress has been made toward using Laue diffraction data for unit-cell determination (Carr, Dodd & Harding, 1993), in earlier studies where structure refinement was performed using Laue diffraction data, the space group and unit-cell parameters were pre-determined using monochromatic X-rays (Helliwell, Gomez de Anderez, Habash, Helliwell & Vernon, 1989; Gomez de Anderez *et al.*, 1989). Solutions to this problem involve unscrambling of the harmonics *via* measurement on multiple films in a film pack (Helliwell, Habash *et al.*, 1989) or direct methods (Hao, Campbell, Harding & Helliwell, 1993) or mathematical deconvolution of data from different crystal orientations (Campbell & Hao, 1993). A second, related problem, is the spatial overlap problem (Cruickshank, Helliwell & Moffat, 1991) in which spots from different crystal planes are sufficiently close together in space to make intensity measurement difficult. An ideal measurement system would allow the intensities of individual components of both types of overlapping spots to be determined.

A further problem is that of wavelength normalization (Helliwell, 1992), in which it is difficult to determine the precise response of a detector for a given energy of the impinging X-rays. Whilst much work has been done to solve this problem when using film, use of other detectors has been limited. These problems could be readily solved by measurement of the wavelength dependence of the detector response and knowledge of the discrete energy or energies of the X-rays producing an individual spot. Access to energy-resolved area detection would allow the Laue experiment to be routinely used for full structure and space-group determinations.

Towards the goal of producing such a detector the use of CIDs for indirect and direct imaging, single photon counting, and possible use as position-sensitive energy-dispersive analyzers, was investigated.

2. Charge-injection devices

2.1. *History*

Charge-injection devices were developed by General Electric Corporation in 1973 (Michon & Burke, 1973) and have been available commercially since 1974. Currently, they are available through CID Technologies, a subsidiary of Thermo-Jarrell-Ash Corporation. Since their introduction, a variety of formats have become available ranging from single-pixel devices of 1 × 2 mm, the CID 75 (Sweedler, Denton, Sims & Aikens, 1987), to 786 × 612 pixel devices, the CID 22 (Zarnowski, Carbone, Carta & Pace, 1994). CIDs have found use as detectors for atomic emission spectroscopy (Bilhorn & Denton, 1989), and commercial instruments incorporating CIDs are available (Thermo-Jarrell-Ash Corporation IRIS). Other applications include: Raman spectroscopy (True, Hanley, Gilmore & Denton, 1994), video imaging in high-radiation environments (Zarnowski, Carbone, Carta & Pace, 1994) and direct detection of X-rays (Fields, Dhez, Slaughter, Falco & Denton, 1992).

2.2. *Architecture*

A CID consists of a two-dimensional array of pixels as illustrated in Fig. 1. Each pixel contains a pair of crossed polysilicon electrodes over an SiO_2 insulating layer covering an *n*-doped layer of epitaxial silicon. The epitaxial layer is 15–38 μm thick and 5 Ω cm^{-1} (Van Gordon & Zarnowski, 1995) and grown on a *p*-doped substrate. Surrounding the crossed electrodes in each pixel is a field-implant oxide which practically eliminates interpixel charge transfer, making CIDs highly resistant to the charge blooming observed in CCDs. One electrode from each pixel is connected to all other electrodes along its row with an aluminium strap. The other electrode is connected to other pixels in its column in a similar fashion. The electrodes are negatively biased such that photo-generated charge is

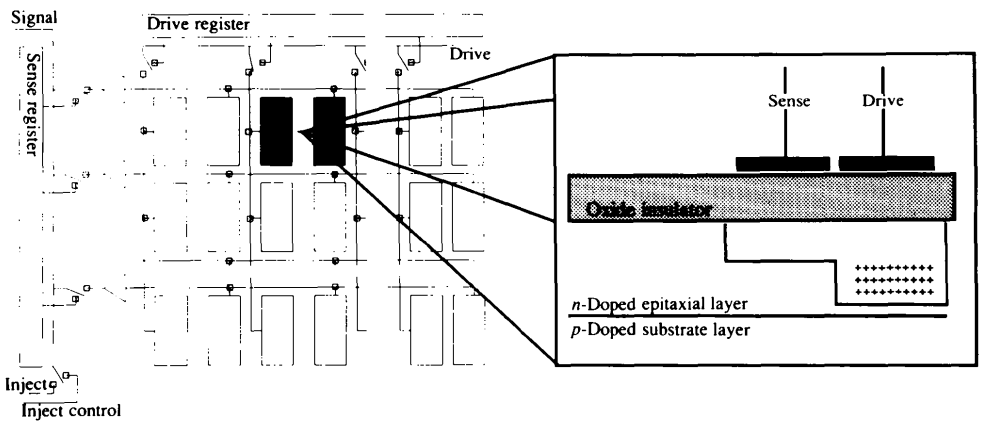

Figure 1
Array architecture of a CID pre-amp per row device. Pixels of a large format array device are addressed using row and column shift registers. Electrodes consist of crossed polysilicon insulated by an oxynitride layer. Individual pixels are isolated by an oxide implant. All the electrodes along a row are connected with an aluminium strap, as are all the electrodes along a column. The row pre-amplifiers serve to give on-chip gain which results in roughly an order of magnitude decrease in device read noise.

collected in the form of holes. Photo-generated charge may be transferred from one electrode to the other in a procedure that is referred to as a 'slosh'. The ability to transfer charge within the pixel forms the basis for reading the device. Each pixel may be addressed individually in a pseudo-random fashion by selecting the row and column by a set of on-chip shift registers. The collected charge is not lost during the readout and a pixel may be read multiple times.

Two devices, the CID 17PPRA and the CID 38SG, are presented here. Both the CID 17PPRA and the CID 38SG incorporate an on-chip pre-amp for each row of the device and are designed for scientific imaging applications. The pre-amp per row architecture has been found to be useful for reducing device read noise by almost a factor of 10 (Michon, 1987); hence its incorporation into scientific grade devices where low read noise is desirable.

2.3. *Readout*

Readout of a CID depends on the change in voltage that occurs when charge is moved in or out of a capacitor. This relationship is given in equation (1),

$$dV = dQ/C. \quad (1)$$

The readout process is illustrated in Fig. 2. Several nomenclatures are in current use to designate the electrodes. CID Technologies refers to *row* and *column* electrodes. Other authors refer to *collect* and *sense* electrodes or *drive* and *sense*. In the pre-amp per row devices, row and sense can always be considered equivalent. Some ambiguity is introduced by the current practice of both collecting and sensing charge with the same electrode. In previous devices either the row or the column could be used for readout or collection and collection of photo-generated charge has been performed with either the row or the column electrodes. To stress the readout mechanism, drive and sense have been adopted here, with the drive corresponding to whichever electrode is not used to sense charge. This usage is slightly different than that found in previous publications but best reflects the device readout used here. During charge collection (Fig. 2*a*) both drive and sense electrodes are negatively biased with respect to the epitaxial layer and the sense electrode is held more negative than the drive electrode. A pixel read is performed after disconnecting the sense electrode from its reference potential. The potential of the sense electrode is sampled before (Fig. 2*b*) and after (Fig. 2*c*) the voltage on the drive electrode is taken more negative than the sense electrode. The change in potential at the drive electrode causes the charge under the sense electrode to migrate to the drive electrode. Following read out of the pixel, the potential on the drive electrode is returned to its original value. To clear accumulated charge in the device the potentials on both electrodes are collapsed (Fig. 2*d*) and charge recombination occurs. It should be noted that readout does not affect the ability of the device to collect charge.

Readout of an individual pixel is performed by selecting the row and column corresponding to the pixel with a pair of on-chip shift registers. This gives the capability of random pixel access. This is in contrast to CCDs in which each pixel must be read in a sequential fashion by first moving the collected charge to a parallel register then to an output amplifier. At present, the on-chip shift registers are unidirectional leading to the current generation of devices sometimes being described as pseudo-random access. The present generation of devices have an approximately 6–100 kHz pixel rate. This is slower than many CCDs, especially compared to CCDs with 20–30 electrons of noise. CCDs of this type can operate well at pixel rates over 1 MHz. The advantage of CIDs is the rapid readout of individual pixels at random locations on the device, without disturbing the collected charge. A CCD must always be exposed for a specified period of time. In a CID the option of exposing the device until a specified signal-to-noise ratio is reached is available.

In comparison to CCDs, CIDs typically have greater full-well capacity and greater flexibility of readout. CIDs have a greater read noise (149 electrons for a single read of a CID 17PPRA *versus* 4–6 electrons for typical scientific grade CCDs). In theory, the read noise of a CID is limited by

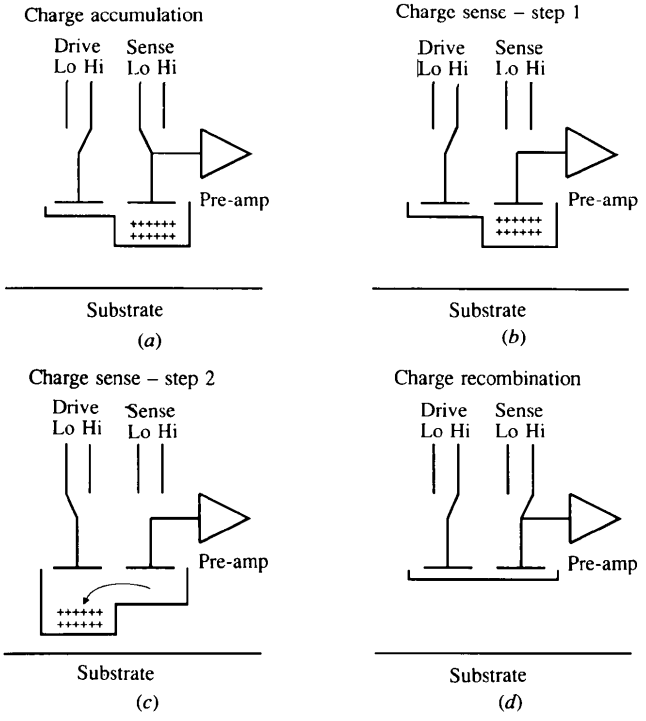

Figure 2
(*a*)–(*d*) Schematic representation of readout in a CID. During charge accumulation and readout the drive high and sense high are held at 6.75 V. The drive low is set to −3.75 V and the sense low is held at 1.5 V. During charge recombination ('injection') both drive and sense are set to 7.70 V. The epitaxial layer is set to 8.19 V. (See text for additional details.) These voltages can be changed. For example, setting the drive low potential 0.6 V lower and sense low potential 0.3 V lower will increase the well capacity somewhat.

row capacitance. Practically, this limit has not been reached and models of CID noise assume that preamplifier noise dominates all other noise sources (Van Gordon & Carbone, 1994). Such considerations place a practical limit of about 110–165 electrons in the CID 17PPRA and CID 38SG. As other sources of noise degrade the signal, a somewhat higher read noise is usually obtained.

2.4. *Nondestructive readout and dynamic range*

Unlike CCDs, which are read destructively, the photogenerated charge collected in the CID imager can be read multiple times, even during image acquisition. If the charge in a pixel is read n times, the error in the measured signal, e_m, can be reduced by the square root of the number of reads as described in equation (2). σ_r is the noise for a single read.

$$e_m = \sigma_r/(n)^{1/2}. \quad (2)$$

Use of multiple reads on each pixel lowers the full frame read rate.

The dynamic range of a CID can be extended beyond the range predicted by the full-well capacity using a process referred to as random-access integration (RAI). RAI involves varying the time of integration for each portion of interest in an image depending on the intensity of the region. Signal levels are monitored during exposure and signal levels recorded when a desired signal-to-noise ratio is reached. Using this technique dynamic ranges in excess of eight orders of magnitude have been demonstrated (Bilhorn & Denton, 1990).

2.5. *Charge injection*

In older CIDs, the amount of charge collected in a pixel was assessed by measuring the amount of charge 'injected' into the pixel after exposure. This was a 'destructive' readout method and has been almost completely replaced by the nondestructive technique. In current use, 'injection' refers to the process of clearing a stored image. Three separate processes are available to perform this operation: global injection, subarray injection and global knockdown. In a global injection, the voltages on all the row and column electrodes are set close to the voltage on the epitaxial layer. This collapses the potential well that confines the charges allowing them to recombine. Subarray injection is similar. Instead of all the row and column voltages being set to near epitaxial voltage, only the voltages of the row and column corresponding to a particular pixel are collapsed. This allows the charge in a single pixel to recombine. To inject a subarray, this process is repeated for each pixel in the subarray. In the case of subarray injection, the time for injection of each pixel is determined by the speed of the shift registers. In global injection, the injection voltages can be held arbitrarily long. Since the process of injection is slightly different, some hysteresis is to be expected between subarray and global injections.

Global knockdown is similar to global injection except that the voltages are set to a level less than that of the epitaxial layer. This voltage may be adjusted arbitrarily within the limitations of the driver electronics. By setting the 'knockdown' voltage the depth of the well under each electrode is temporarily changed. If the well depth is no longer large enough to hold all of the trapped charge the remainder recombines. The result is to clear all pixels containing more than a selected amount of charge.

Injection voltages must be selected judiciously. If the global injection voltage is set too close to that of the epitaxial layer, it can release charge confined to surface trap sites. Depletion of trap sites results in a 'foot' or 'fat zero' in the response function of a CID. If the voltage is set too far from that of the epitaxial layer, global injection behaves like a global knockdown and ghost images will be observed after injection. This latter effect is particularly evident at liquid-nitrogen temperature.

2.6. *Detection of X-rays*

CIDs can be used for both indirect and direct detection of X-rays. For indirect detection, the X-ray photon is converted to visible light with the use of a phosphor. The phosphor can be followed by a micro-channel plate, fiber optic taper, or a lens prior to conversion of optical photons to charge in the CID. For direct detection, X-rays are allowed to interact directly with the CID. This process results in the creation of multiple hole pairs for each X-ray photon. Replacement of CCDs in indirect X-ray imaging applications with CIDs will allow for the collection of high dynamic range images with the additional advantages of resistance to charge blooming, nondestructive readout, pseudo-random pixel access, selective pixel reset and random-access integration.

For direct detection of X-rays, CIDs offer the possibility of high-speed, position-sensitive, energy-dispersive area detection which is currently unavailable in any other detector. Although this possibility is not completely developed here, data are presented showing the basis for such an energy-dispersive detector. CCD systems have been described which perform similar functions (Janesick, Elliott, Bredthauer, Chandler & Burke, 1988; Lumb, 1990) but the destructive readout of CCDs makes the approach described here impossible. The inability of a CCD to read out individual pixels randomly would require extremely high frame rates, and 0.018 photons pixel^{-1} frame^{-1} has been given as a practical limit in CCDs (Lumb & Nousek, 1992). Devices with active pixels (Beker *et al.*, 1993; Delpierre *et al.*, 1992) could also be developed with the capability of measuring position, energy and intensity. Such detectors are at an early stage of development at present and will remain prohibitively expensive for the immediate future.

3. Experimental

3.1. *Device characterization*

Characterization of the devices used in this report was performed using the method of mean variance to measure

Table 1
System operating conditions.

	Indirect imaging	Direct imaging	Photon counting
CID type	CID 38SG	CID 17PPRA	CID 17PPRA
CID gain parameter[a]	100	100	240
Pixel frequency (kHz)	20	20	9.43
Read noise (electrons)[b]	178	140	190
System gain (electrons ADU^{-1})	80.6	53.2	23.7
Temperature control	Liquid N_2	Liquid N_2	Liquid N_2
Phosphor	Min-R	None	None
Lens	Nikon 50 mm *f*1.8	None	None
Window material	CaF_2	Mylar	Mylar
Read type	Full frame Single read	Full frame Single read	Single pixel 15360 reads
X-ray source	Enraf–Nonius FR571	Enraf–Nonius FR571	Enraf–Nonius FR571[c]
Anode material	Molybdenum	Molybdenum	Molybdenum
Anode voltage (kV)	50	50	50
Anode current (mA)	100	50	50
Beam diameter (mm)	0.2	0.2	0.2
Integration time (s)	0–240	0–30	0–2[d]

(*a*) Gain parameter, GP, and pixel frequency in kHz, PF, are related by the equation: PF = 1000/(10 + 0.4GP). (*b*) CID read noise depends on the pixel frequency as shown in Fig. 4(*b*). See also note (*a*), Table 3. (*c*) A Phillips source with a copper target was also used for single photon measurements. (*d*) Integration time for photon counting refers to the time of sampling. The pixel is sampled 15360 times during this integration period.

Table 2
Crystal test materials.

	Indirect imaging[a]	Direct imaging	Photon counting
Crystal	Tetraphenylphosphonium tetrachlorooxomolybdenum(V)	MoS_2, naturally occurring	MoS_2, naturally occurring
Orientation	Random	Beam parallel to *c*	Beam parallel to *c*
Crystal space group	*P4/n* (Carducci, 1994)	$P6_3/mmc$	$P6_3/mmc$
Unit-cell parameters (Å)	a = 12.7306 c = 7.6845 (Carducci, 1994)	a_0 = 3.1604 b_0 = 12.295 (Wyckoff, 1963)	a_0 = 3.1604 b_0 = 12.295 (Wyckoff, 1963)

All data were collected using Laue geometry and the unfiltered 'white' beam from the FR571. (*a*) The linearity of the indirect camera system was assessed using MoS_2 under conditions identical to those used here for direct imaging.

system gain and read noise (Mortara & Fowler, 1981; Sims & Denton, 1987*b*). Fixed pattern noise is excluded from these measurements by the use of two exposures of the same subarray for each level in the mean-variance measurement (Sims, 1989). Variance is then computed on the difference between the subarray images. Knowledge of the system gain allows the quantum efficiency to be measured. A NIST traceable photodiode reference was used (UV-444-BQ, EG&G) to calibrate the light source for measurements of quantum efficiency (Sims & Denton, 1987*b*). The UV–visible characterizations are generally applicable to any system that would use these devices for *indirect* detection of X-rays. Device random access was tested using 10 000 randomly positioned pixel reads at four gain settings. All characterizations were performed with devices operated with liquid-nitrogen cooling.

3.2. *Indirect imaging*

Indirect imaging of diffraction patterns used a CID 38SG device installed in a commercially available camera system (Van Gordon, Hutton, Fassett & Carbone, 1993) (SiCAM, CIDTEC). This camera consists of a vacuum Dewar for cooling the detector to liquid-nitrogen temperatures. The indirect imaging system consisted of a 50 mm lens (Nikon) and a MIN-R (Kodak) medium X-ray phosphor. This camera was installed on the base of a modified precession camera (Enraf–Nonius) and attached to one port of an Enraf–Nonius FR571 rotating-anode X-ray source with a molybdenum anode. The unfiltered direct beam was used to generate the Laue diffraction pattern. The system operating conditions were as outlined in Table 1. The crystal systems used to demonstrate indirect imaging are reported in Table 2. A block diagram of this apparatus is illustrated in Fig. 3(*a*). Linearity was assessed by measuring the charge accumulated in areas corresponding to both strong and weak diffraction spots as a function of the time of illumination.

3.3. *Direct imaging*

Direct imaging was performed using a CID 17PPRA device installed in a custom-designed camera system. A liquid-nitrogen Dewar (IR Laboratories, Tucson) fitted with a 0.005 in Mylar window allowed for passage of X-

rays while providing a vacuum seal for the Dewar. An additional layer of black plastic covered the Mylar window to block visible light. The camera system was mounted on the base of the precession camera described above. The Enraf–Nonius FR571 rotating-anode X-ray source employed for indirect imaging was used as a source for the generation of the Laue diffraction pattern. Single photon counting measurements were made on selected reflections from the Laue pattern of naturally occurring MoS_2 and using a Philips X-ray source with a copper target. No physical changes are required to use this direct camera for photon counting. The main difference in approach is that instead of a full frame read a single pixel is repeatedly read. The system conditions used for direct imaging and photon counting are summarized in Table 1. The crystal systems used to demonstrate direct detection and photon counting are presented in Table 2. Fig. 3(*b*) gives a block diagram of this camera system.

Since photon counting is performed by repeatedly reading a single pixel during charge accumulation, a derivative is computed to observe single photon events. Here, the derivative is computed on a 50-point moving average. As indicated by equation (2), this lowers the measurement noise by a factor of 7. Conversion of measurements made in ADU (arbitrary digital units) to energy values in eV were made using measured system gains in carriers per ADU and the average energy required to generate an electron hole pair in Si (3.65 eV). Single photon counting used a discriminator set to approximately 150 eV. Single events greater than this value were counted and the event height measured. This corresponds to a single-event height of slightly less than 2 ADU at a CID gain parameter setting of 240.

Radiation-damaged devices were annealed in a vacuum oven at 453 K for 8 h.

Images presented in this work were generated with *IRAF* (National Optical Astronomy Observatories, Tucson), running on a SparcStation II (Sun Microsystems).

Table 3
CID data and characterization summary.

Parameter	CID 38SG	CID 17PPRA
Pixel dimension (μm)	28 × 28	28 × 24
Device format	512 × 512	256 × 388
Active area	1.96 cm^2	6.948 × 9.120 mm
Single read noise (electrons)[a]	178	140
Read noise, 100 NDROs (electrons)	24.4	15
Read noise, 1000 NDROs (electrons)	6.8	4.5
Full-well capacity (electrons)	10^6	10^6
Dark current (electrons pixel s^{-1})	<0.1	<0.1
Maximum quantum efficiency (optical) (%)	57	45
System gain (electrons ADU^{-1})[a] Gain parameter = 100	80.6	53.2
System gain (electrons ADU^{-1})[a] Gain parameter = 200	47.1	30.5
Pixel rate (kHz) Gain parameter = 100	20.0	20.0
Pixel rate (kHz) Gain parameter = 200	11.1	11.1

(*a*) Values for single read noise reported here are for the camera systems used in these experiments. These values vary depending on the readout electronics used. The system gains and device full-well capacities also reflect the particular readout electronics and operating voltages used and should not be taken as constants for these devices.

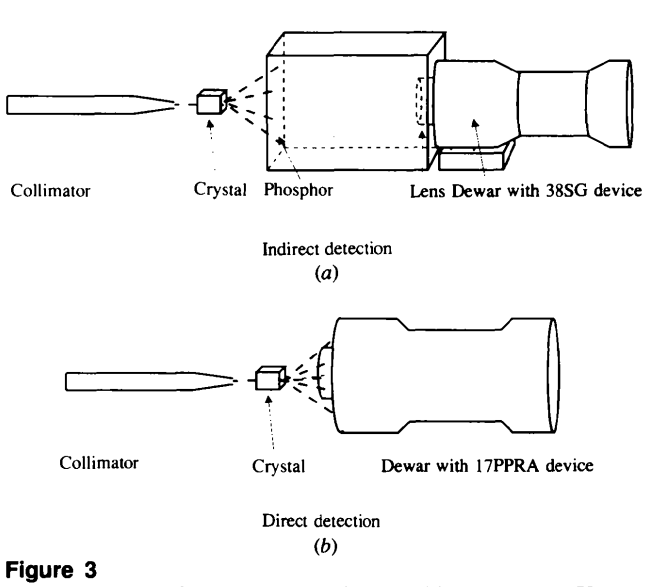

Figure 3
(*a*) System used for indirect imaging. In this system the X-rays generate optical photons after striking the MIN-R phosphor and are imaged using a lens. The 38SG is installed in an evacuated Dewar with liquid-nitrogen cooling. The focused light passes through a CaF_2 window before reaching the active surface of the CID 38SG. The readout electronics are not shown. The Dewar, window and readout electronics are as supplied with the SiCAM system by CID Technologies. (*b*) System used for direct imaging. In this system the quartz window, lens and phosphor are removed and replaced with a 0.005 in Mylar window. This allows most X-rays to pass through the window where they strike the 17PPRA device. The number of carriers generated per arriving X-ray photon depends on the energy of the incident X-ray. The Dewar, window and readout electronics were assembled or modified in these laboratories and have slightly higher system gain than is found in the standard SiCAM camera system. For most purposes direct detection can be performed with the standard instrument after replacement of the quartz window with 0.005 in Mylar.

4. Results

4.1. *Device characterizations*

Characterizations of the devices used in this report are summarized in Table 3. The values obtained for system gain, read noise, full-well capacity and quantum efficiency are consistent with other characterizations performed on CID devices in these laboratories. Fig. 4(*a*) shows the relationship between the single-pixel read rate for 10 000 randomly positioned pixels, the number of nondestructive readouts (NDROs) and the gain parameter. Fig. 4 indicates that selected regions of the device can be read at rates much higher than would be possible for a CCD of similar size. The read-noise and system-gain parameters for the CID 38SG are presented in Figs. 4(*b*) and 4(*c*), respectively. The decrease in measurement error, e_m, as a function of the number of NDROs for the same 38SG device is presented in Fig. 4(*d*).

4.2. *Indirect imaging*

Fig. 5 shows a series of Laue diffraction patterns generated by tetraphenylphosphonium tetrachlorooxomolybdenum(V) in a random orientation. The first image (Fig. 5*a*) shows a typical diffraction pattern from this crystal. In the second image (Fig. 5*b*) a streak extending the full width of the device appears along the row axis. This is due to row cross-talk. Cross-talk is seen in this device when some of the pixels along a row have reached saturation and has been noted previously (Sims & Denton, 1987*a*). Under most conditions this behavior has been eliminated; however, it may be present when many pixels along a row have reached saturation. In the image shown here the effect is small representing about 20 ADU (approximately 2000 carriers). The appearance of row cross-talk can be removed from an acquired image by the application of a gradient filter. This is shown in Fig. 5(*c*) in which the gradient has been computed along the row axis. In Fig. 5(*b*), the gradient is computed at a 45° angle to the *y* axis.

Table 4 summarizes linearity data from a series of images of MoS_2 as a function of the time of exposure for selected spots. These data are shown plotted in Fig. 6. The nondestructive readout of the CID 38SG was used to record the data presented in Table 4. Each successive image included the charge accumulated during the previous period of exposure. The large deviations from linearity in the peaks of lowest intensity are due to a 'fat zero' in the response function of the CID 38SG. This is a characteristic of surface-channel charge-transfer devices and has been noted previously in CIDs (Sims & Denton, 1987*b*). The 'fat zero' is caused by trap sites at the Si/SiO_2 interface. In the reflections with greater intensity, the majority of the

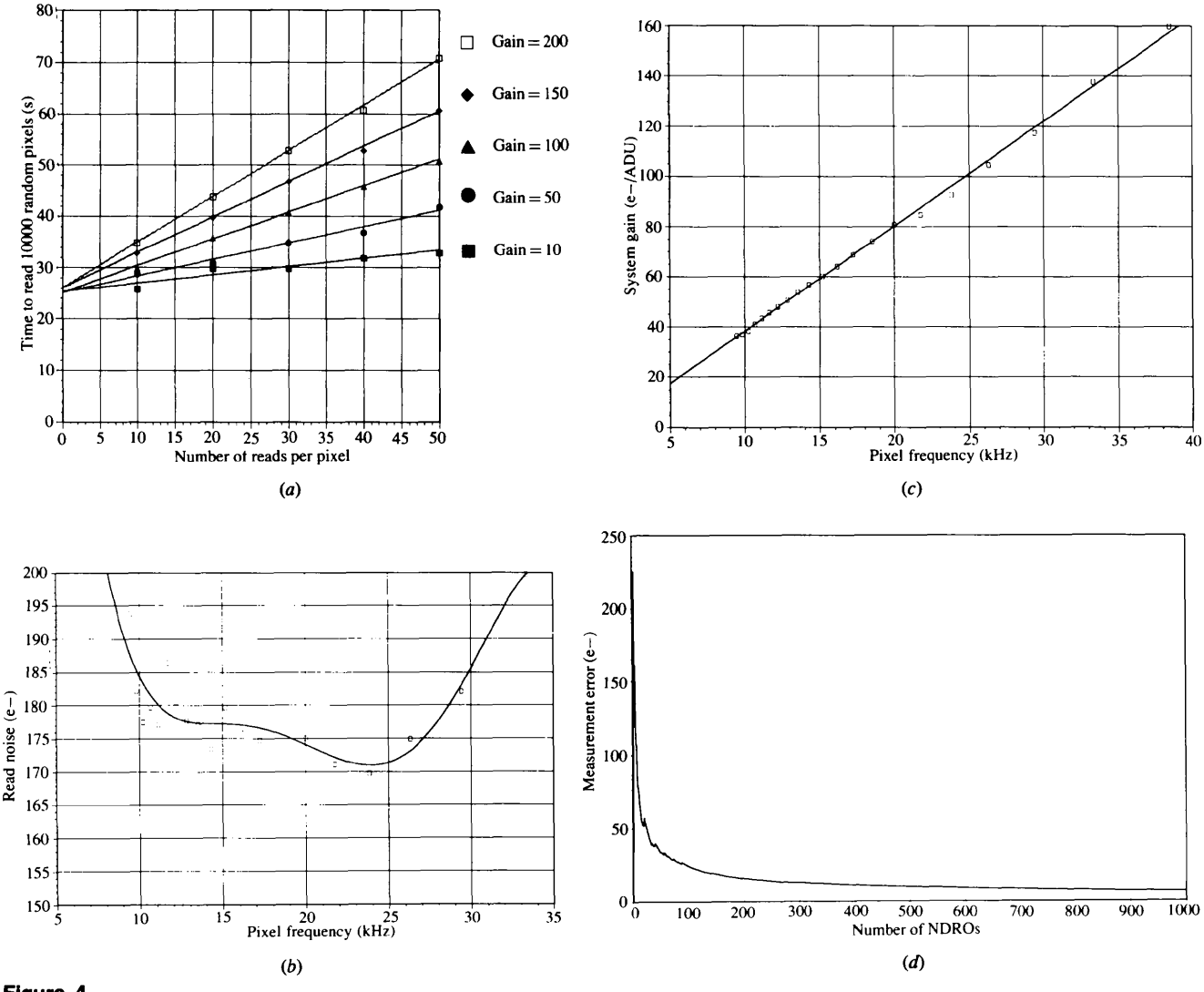

Figure 4

(*a*) Data showing read rates for 10 000 randomly positioned pixels on the CID 17PPRA device. Data were taken at gains of 10, 50, 100, 150 and 200. The number of re-reads for each pixel varied from 10 to 50. The maximum read rate at a gain of 100 was 25 000 s^{-1} with 100 reads per randomly positioned pixel. Read noise (*b*) and system gain (*c*) as a function of pixel read rates for a CID 38SG. (*d*) Reduction in measurement error as a function of the number of NDROs.

deviations from linearity appear to be the result of variation in beam intensity over the period of exposure. Residuals analysis of the data for reflections *A*, *B* and *C* showed that each demonstrated a similar positive deviation for time points 6 and 7 (804 and 1150 s, respectively) suggesting an instability in the incident beam. Regression of *A* and *B* against each other, presented in Table 4, shows clear improvement. Pre-amp per row CIDs have been shown to deviate from linearity when approaching full well (Pilon, 1991). This deviation may be corrected by application of a second-order correction applied to the raw data, but no correction was applied to the data in Table 4. In the image with longest exposure, the ratio between spots of highest and lowest intensity is 840.

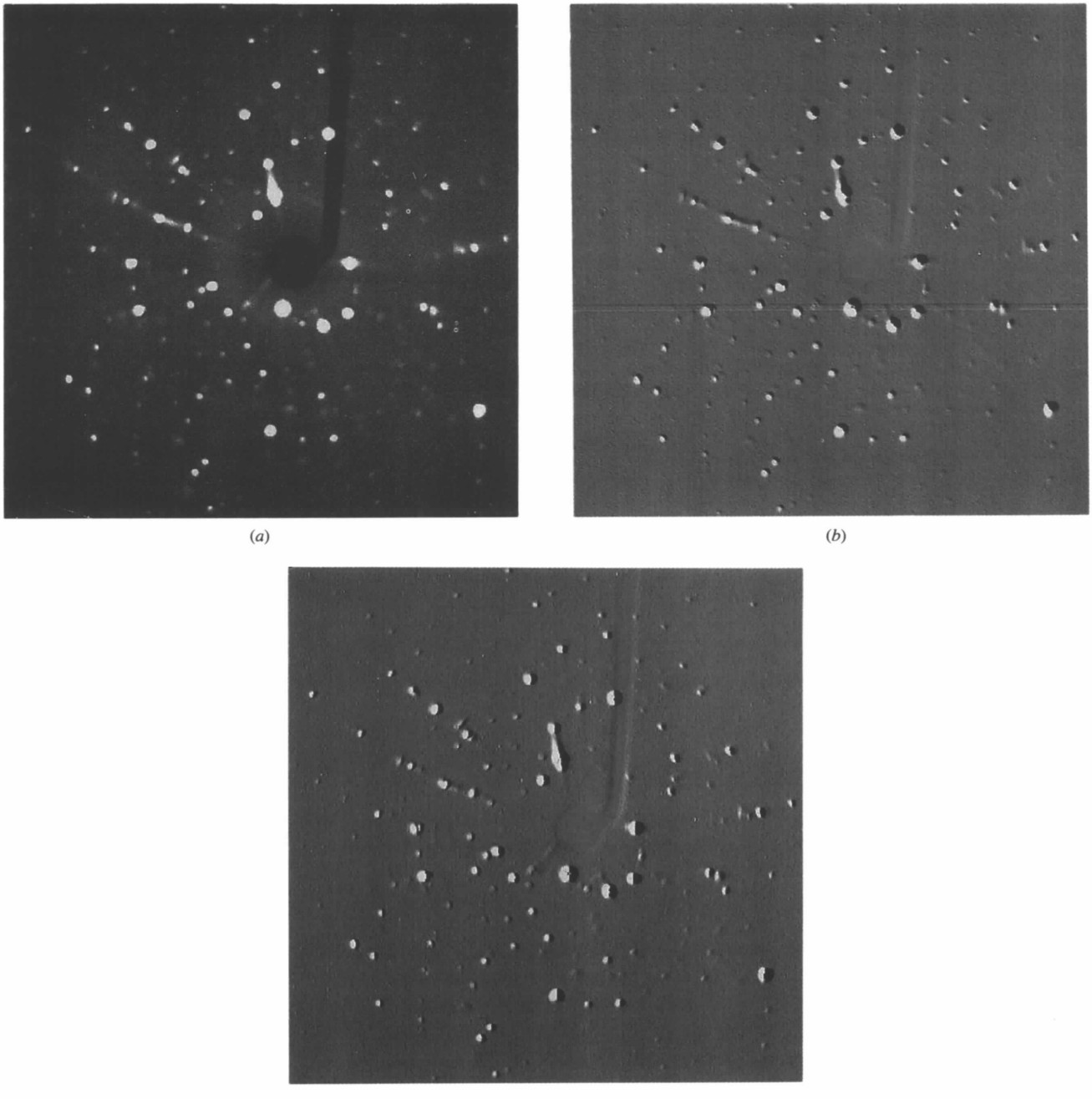

Figure 5
Indirect Laue diffraction pattern of tetraphenylphosphonium tetrachlorooxomolybdenum(V) imaged using the CID 38SG device. (*a*) The image after 843 s of exposure. (*b*) The same image after further exposure showing the development of row cross-talk. This figure is shown using gradient filtering to allow easier visualization of the cross-talk. The cross-talk appears as a streak extending the length of the *x* axis and is roughly six pixels high. Saturation of the brightest reflections has occurred along these rows. (*c*) The same data presented in (*b*) except with the application of the gradient along the row axis. This effectively removes all the observed cross-talk. In (*b*) the gradient was computed at a 45° angle to the *y* axis.

Table 4
Linearity for indirect detection.

Reflection	Slope (ADU s^{-1})	Intercept (ADU)	R^2	Linearity (%)[a]
A	396.3 ± 7.7	691 ± 6320	0.997	1.9
B	262.0 ± 4.4	804 ± 3627	0.998	1.6
C	76.3 ± 1.2	−773 ± 998	0.998	1.6
D	5.12 ± 0.20	−271 ± 164	0.990	3.9
E	0.425 ± 0.09	−123.2 ± 73	0.790	21
A vs B	0.6614 ± 0.0044	415.5 ± 1426	0.9997	0.6

(*a*) Linearity is expressed as the standard error divided by the slope.

4.3. *Direct detection*

Fig. 7 shows a direct image of a portion of the diffraction pattern of MoS_2. Fig. 8 shows linearity data for the direct detection of X-rays from MoS_2 Laue diffraction. In these exposures, no 'fat zero' was seen and the linearity was slightly better than in the indirect images acquired using the CID 38SG. The better linearity is thought to be the result of the shorter exposure times employed in these experiments (0–30 s). The absence of the 'fat zero' in the response function of the CID 17PPRA used here is largely due to the large number of carriers generated for each X-ray photon.

Fig. 7 also shows a section of the device that has been damaged by exposure to X-rays. This section appears in the lower left side of the image and is unresponsive. It should be noted that this region does not affect the response of the remainder of the device. This reflects the architecture of the CID, in which charge is read in place rather than moved to a register for readout. The damage to the CID 17PPRA device was the result of exposure to the direct unfiltered beam from the rotating-anode generator. Best estimates of the radiation dose based on ion-chamber readings of the beam indicate this region received 50 000–100 000 rad. At present these values should be considered estimates since the exact length of exposure is unknown (15–30 min) and the ion-chamber readings from the white beam are approximate (200 000 rad h^{-1}). Annealing in a vacuum oven at 453 K for 8 h allowed the insensitive region indicated in Fig. 7 to become responsive to light. Annealing of the devices resulted in a change in device fixed pattern.

4.4. *Single photon counting*

Fig. 9(*a*) presents raw data showing a portion of a set of 15 360 reads of a single pixel during exposure to X-rays from a reflection from naturally occurring MoS_2. The 15 360 reads took 2 s to complete. Several events are clearly visible in the set of reads, appearing as steps in the amount of charge collected in the pixel. The 47 events observed in this figure correspond to approximately 5×10^6 photons cm^{-2} s^{-1} detected by the CID. Fig. 9(*b*) shows a similar set of reads from the same pixel with the X-ray shutter on the rotating anode closed. No events were seen in this set of reads and no general upward trend in the data was seen. Figs. 9(*c*) and 9(*d*) show these data plotted as a derivative to emphasize the steps corresponding to X-ray-induced events. Fig. 10 shows peak heights plotted in

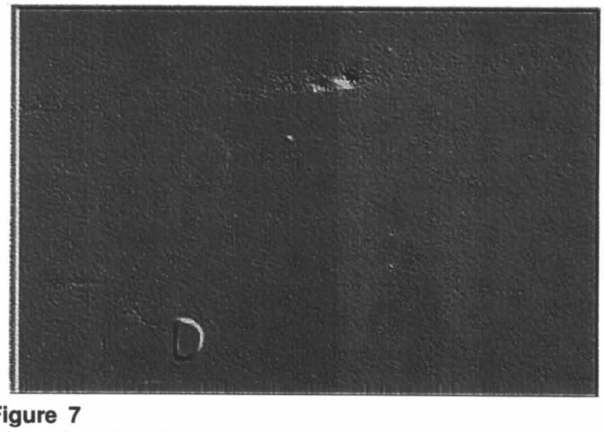

Figure 7
Direct detection of a reflection from MoS_2 using the CID 17PPRA device. A localized region of damage from the direct beam of the rotating anode appears in the lower left portion of the device.

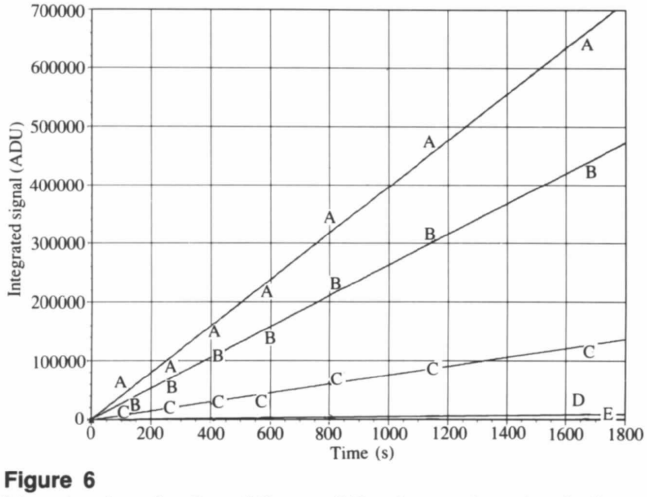

Figure 6
Linearity data for five different diffraction peaks using indirect detection with the CID 38SG device.

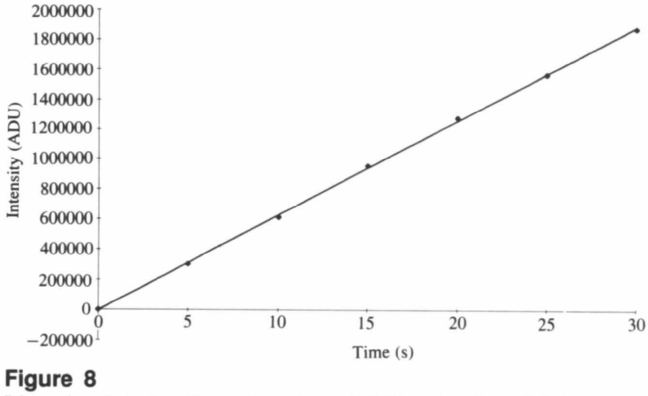

Figure 8
Linearity data for direct detection of diffraction from MoS_2 using the CID 17PPRA. The maximum time of exposure was 30 s. Overall linearity was 0.8%.

the form of a multi-channel analyzer while the device was being exposed to Cu $K\alpha$ radiation. This figure indicates that roughly 25% of the charge produced by a Cu $K\alpha$ photon is collected in a single pixel. The events observed in a similar series of reads are plotted in the form of a multichannel analyzer in Fig. 10. Figs. 9 and 10 show several limitations of the CID 17PPRA when operated as a photon counter with energy discrimination. Much of the charge collected in the pixel is the result of interactions below the 150 eV threshold of the discriminator. Two factors account for this behavior: incomplete charge collection and split events in which the X-ray-generated charge is collected in several pixels. Both of these effects have been observed in CCDs used in similar fashion (Janesick, Klaasen & Elliott, 1987).

5. Discussion

5.1. *Indirect imaging*

Several features of CIDs recommend their use for area detection of indirect diffraction pattern images. These are: the large full-well capacity, the selective nondestructive readout, real-time evaluation of image quality and selective detector reset, all of which combine to give a wide dynamic range. With fixed exposure time and a single read of the CID 38SG, a maximum dynamic range of 3000 is possible assuming the minimum detectable charge accumulation in a pixel is twice the single read noise of the device. The value of 840 measured here is roughly 1/4 of this value. This dynamic range can be extended by using the RAI and NDRO capabilities of CIDs. An example of showing how a dynamic range of 10^8 may be obtained is given in Table 5. Such a wide dynamic range is very difficult to obtain using a CCD and may be impossible if the strong and weak peaks are present in the same row or column of the CCD. The CID gives the capacity to accumulate continuously until a suitable signal-to-noise ratio has been reached.

Table 5
Dynamic range calculation

	Peak *A*	Peak *B*
Charge accumulation rate (electrons s^{-1})	10^7	0.1
Integration time (s)	0.05	2000
Signal (electrons)	0.5×10^6	200
NDROs	1	100
Read noise[a]	180	18.0
Dark current noise (electrons)	<1	14
S/N[b]	1390	3.1

(*a*) These values have been adjusted according to equation (2). (*b*) *S/N* here is given as the measured signal divided by twice the read noise.

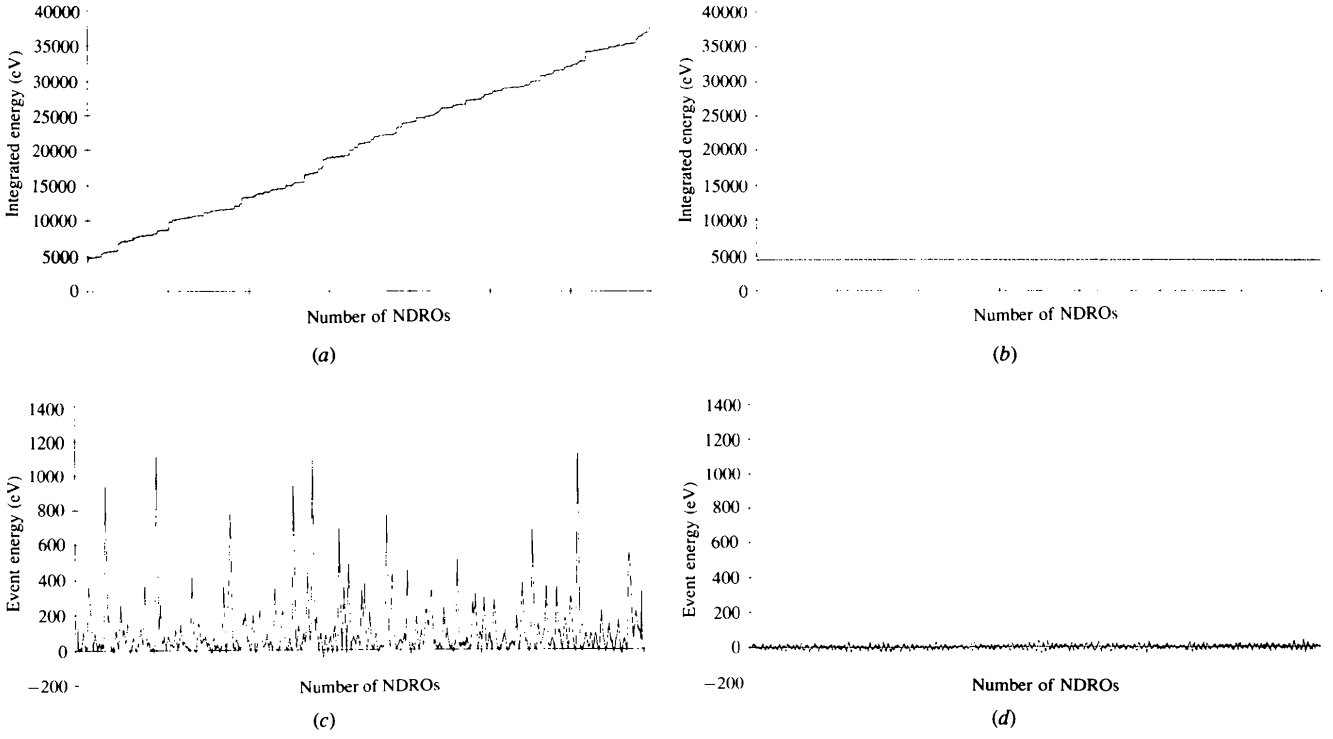

Figure 9
(*a*) 15 360 reads from the pixel at position (25,15) of the CID 17PPRA while the X-ray source was on. This position contained a portion of a reflection from MoS_2. This set of reads shows a gradual increase with steps from X-ray interactions superimposed. (*b*) 15 360 reads from pixel position (25,15) of the CID 17PPRA with the X-ray source off. This set of reads shows no equivalent increase to that seen in (*a*). (*c*) The 50-point smoothed derivative of the curve shown in (*a*). The energy axis is computed from the system gain parameter and the direct band gap energy for Si (3.65 eV). The maximum event height observed in this set of reads is 1200 eV. (*d*) The 50-point smoothed derivative of the curve shown in (*b*) demonstrating the absence of X-ray events. Maximum deviation from 0 is less than 50 eV.

The use of CIDs for indirect detection of X-rays has some significant limitations. While they do not have the charge-blooming problems of many CCDs, care should be exercised using CIDs under saturating conditions. The devices are not linear when approaching full-well capacity, and, under highly saturating conditions, eventually show a decreasing signal with increasing exposure. For best results with X-rays, a polynomial correction should be applied to the raw data to obtain a linear response. In CCDs, saturation of the device can lead to charge blooming to adjacent pixels. While CIDs rarely show charge blooming, when operated under saturating conditions they do show row cross-talk. Cross-talk is to be distinguished from the charge blooming seen in CCDs. Charge blooming in CCDs causes charge to migrate from a heavily exposed pixel to adjacent pixels in both the row and column directions. Unless the entire row or column is saturated, charge does not spread uniformly. In contrast, cross-talk in CIDs is confined to the row direction, never appearing in both row and column directions, and affects all pixels along the row uniformly. Cross-talk can be removed from an acquired image by the use of a gradient filter computed along the row axis. The use of gradient filtering is satisfactory in this case because the cross-talk appears exclusively along the row axis of the device and affects all pixels along the row equally. If it were charge blooming, gradient filtering would be ineffective. Gradient filtering results in some loss of information and will add to data reduction, but should prove satisfactory for most purposes as seen in Fig. 5(*c*). Cross-talk and device saturation occur under conditions outside the well capacities of comparable CCDs and, since CIDs can be read nondestructively during data acquisition, conditions causing these effects can be easily avoided. If cross-talk is observed in an image prior to destruction of the acquired image, the saturated pixels can be selectively reset and the image re-read.

The 'fat zero' noted here is a characteristic of surface-channel charge-transfer devices. At the Si/SiO_2 interface of a CID or surface-channel CCD a large number of energy states other than the conduction and valence bands of Si are available to hold charge. These 'trap' sites are located in a fixed location in the device and can exchange charge with time constants ranging from microseconds to hours (Sims & Denton, 1987*b*). When charge injection is performed to clear charge from a CID, these trap sites can be depleted. Subsequent exposure will generate charge that will initially fill these sites. Charge confined to trap sites is immobile and not measured during the readout process. This results in a so called 'fat zero' or 'foot' in the response function of the device. Discussion of the 'fat zero' here is primarily precautionary, since strategies are available to eliminate the problem. Using a procedure similar to 'pre-fogging' of film, the CID can be exposed to sufficient light to fill the trap sites with charge. Subsequent use of the re-read capability allows the effects of uneven illumination during this exposure to be eliminated. Alternately, the 'knockdown' feature of the CID can be employed to assure that trap sites are not depleted when the device is cleared (Van Gordon, Hutton, Fassett & Carbone, 1993).

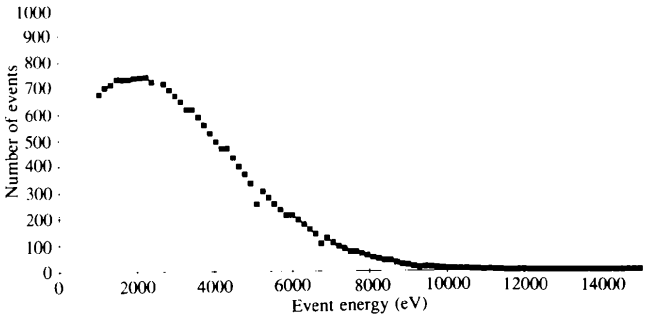

Figure 10
Histogram of events from multiple reads of the CID 17PPRA during exposure to Cu $K\alpha$ radiation. Although single photon events are readily seen, energy analysis is hindered by incomplete charge collection in a single pixel. The figure indicates that roughly 25% of charge is collected in a single pixel.

5.2. *Direct imaging*

Many of the advantages discussed in relation to indirect imaging apply here: the large full-well capacity, the selective nondestructive readout, real-time evaluation of image quality and selective detector reset. There are a number of important drawbacks to the use of these devices in direct imaging, most of which are shared with CCDs: lowered dynamic range, small device formats and radiation-induced damage. Even with a well capacity of 10^6 electrons, assuming complete charge collection, 450 Cu $K\alpha$ photons in a single pixel will saturate the pixel. CCDs share this disadvantage. With a present maximum active area of 1.96 cm^2 for the CID 38SG, applications using a small beam diameter and a short crystal-to-detector distance are possible. Devices with four times the number of pixels and active area of the CID 38SG are being developed, but the utility of these devices for direct detection of X-rays from diffraction is limited.

Radiation exposure to scientific grade CCDs has been reported to cause degradation resulting in high dark current, voltage shifts, increased surface states, lowered charge-transfer efficiency and bulk damage (Roy, Watts & Wright, 1989). Some of this damage can be reversed by annealing with heat (Herve, Lefesvre & Dupont-Nivet, 1992), intense UV radiation (Acton, Morrison, Janesick & Elliott, 1991), or heating in the presence of forming gas (Allinson, Allsopp, Quayle & Magorrian, 1991). CIDs show similar behavior. Although CIDs are expected to be more resilient due to the lower charge-transfer efficiency requirements for readout, they are not indestructible as seen in Fig. 7. At present the behavior of scientific grade CIDs during radiation-induced degradation is not known and further work is being performed at present. A specialized CID has been shown to withstand in excess of 10^6 rad when evenly exposed (Zarnowski, Carbone, Carta & Pace, 1994). In the study on the specialized devices, the clock voltages

of the imager had to be adjusted to compensate for FET gate threshold shifts. The uneven voltage shifts produced from uneven exposure to X-rays will prove harder to compensate for than those produced during even exposure, a problem shared with CCDs. The level of radiation tolerance demonstrated in the specialized device has not yet been achieved in a scientific grade device. Both the CID 38SG and the CID 17PPRA devices were optimized for use in optical spectroscopy, not X-ray detection. Even without such optimization the CID 17PPRA showed good resilience when exposed to high X-ray fluxes, performing up to approximately 50 000 rad. While some of this damage can be reversed by annealing, the long-term behavior of annealed devices needs to be investigated in more detail as does the behavior of these devices under direct X-ray exposure.

5.3. *Single photon counting*

One of the unique uses of a CID is for single X-ray photon counting. CIDs can be used as position-sensitive energy-dispersive analyzers, provided the *collected* charge reflects the *generated* charge. Although CIDs will have a limited lifetime in the presence of high radiation and the active area is relatively small, they have the potential to operate at higher fluxes than do present CCDs. Figs. 9 and 10 show the strategy for using CIDs as energy-dispersive detectors and also show the limitations of the present devices for this purpose. The shape of the curve in Fig. 10 is similar to CCDs with low charge-collection efficiency (Janesick, Klaasen & Elliott, 1987). Additionally, CIDs have a greater read noise than does a CCD. Construction of Fig. 10 required the use of multiple NDROs of the CID 17PPRA and could not be done with single reads. If a larger number of contiguous pixels are observed in order to sum the charge collected from split events, the high read noise of the CID becomes a limiting factor. For example, using the 178 electrons of noise measured for the 38SG, a total of about 250 electrons of noise can be expected after taking the difference between the charge in a pixel before and after an X-ray event is observed. This translates into almost 1 keV uncertainty in the energy of the incident photon. While some of this uncertainty can be removed by the use of multiple re-reads, as has been done here, this reduces the speed of the measurement. For example, to reduce the uncertainty in the photon energy to about 100 eV, 80 reads or more must be employed resulting in a lower effective readout rate. At these lower read rates, the only present advantage of CIDs over commercially available CCDs for this purpose is a lower sensitivity to radiation-induced reduction in charge-transfer efficiency. The readout rate can be increased in the current generation of devices by almost an order of magnitude with only a negligible increase in read noise, an active area of research in these laboratories. In practice, as seen in Fig. 10, it is rare that all the charge produced from an interacting X-ray photon is collected in a single pixel. This increases the difficulty of locating and measuring the X-ray generated charge. If a three by three array of pixels is sampled, the number of reads required increases accordingly. Signal-to-noise expressions become complicated under these conditions and full treatment is beyond the scope of the present paper. Although promising in this application, the energy-dispersive resolution of the CIDs investigated here is poor and methods to improve it are under investigation.

CCDs used for photon counting operations have an upper count rate limit of 0.15 photons pixel^{-1} frame^{-1} for single-pixel events and about 0.018 photons pixel^{-1} frame^{-1} for events spread over multiple pixels (Lumb & Nousek, 1992). Using a 7.5 kHz single-pixel read rate and similar considerations, CIDs have a maximum count rate of 1130 photons pixel^{-1} s^{-1} for events corresponding to greater than 5 keV. This assumes 10 times read noise for the event height and single reads. For lower energy events, this rate will be reduced by the number of re-reads required to obtain a suitable signal to noise. It should be noted that CCDs and CIDs are very different in this capability. CCDs can be used as true multi-channel photon counters, a use that is limited by the high read noise of the CID. CIDs operated as described here are sequential instruments capable of higher count rates in a single pixel. A device with a pixel rate of 500 kHz, currently under development, should be able to reach rates of 15 000 photons pixel^{-1} s^{-1}.

As noted earlier, the devices studied here were optimized for optical spectroscopy. Several approaches can be taken to optimize the X-ray response of the devices. The first is to apply the techniques used for radiation hardening CIDs in other applications to the scientific grade of CIDs. For use in energy-dispersive detectors, CIDs can be constructed of high-resistivity silicon allowing for deep depletion regions to capture charge from deep events better. A second unique possibility for CIDs is the construction of a deep insulator or virtual phase between pixels. A deep implant insulator would electrically isolate pixels allowing charge generated deep in the device to be confined better to the pixel in which it was created. A virtual phase could also be used to repel charge carriers away from the edges of a pixel actively. In a CCD, these options would be limited since the charge must be moved out of the pixel before readout.

6. Conclusions

CIDs are highly versatile detectors that can be placed roughly midway between image plates and CCDs. CIDs can be read more rapidly than an image plate but at present have somewhat lower spatial resolution. CIDs can compete with image plates for dynamic range using RAI, but this requires real-time analysis during data collection, which can be difficult to implement. CCDs generally have faster readout and lower noise than CIDs. For this reason, CCDs are better suited to indirect low-signal imaging applications than are presently available CIDs.

CIDs may be used for direct imaging applications. There are applications where this might be of some utility such

as alignment of X-ray beams, but is not generally useful for diffraction applications. Radiation damage to the CIDs investigated here was a problem and a more comprehensive study of annealing of CIDs remains for the future.

Single photon counting with CIDs is an interesting variant of methods already in use in CCDs. At present the energy resolution is poor, but the high count rates CIDs are capable of measuring make them interesting for future work in this area.

For Laue diffraction, the primary attraction of the CID is its wide dynamic range when using RAI methods and indirect detection. Future devices may be able to measure the energy or energies of single diffraction spots at count rates suitable for Laue diffraction applications. Such devices, however, are not currently available. As presented here, the full potential of CIDs for both monochromatic and Laue diffraction applications has not been reached.

The long-term goal of this research is to develop instrumentation that can resolve the energies of individual spots within a Laue diffraction pattern. The problems that must be solved before Laue diffraction data can be used for routine analysis of molecular structures have been reviewed by several workers (Coppens, 1992; Helliwell, 1992). The full use of Laue diffraction data requires that all the components in equation (3) be evaluated.

$$I(\mathbf{h}) = (e^2/mc^2)^2(\mathrm{d}I/\mathrm{d}\lambda)\lambda^4(1/2\sin^2\theta)(V/V_0{}^2)PAD|F(\mathbf{h})|^2 \quad (3)$$

where $I(\mathbf{h})$ is the intensity of a reflection, $\mathrm{d}I/\mathrm{d}\lambda$ is the spectral intensity distribution of the incident X-ray beam, V is the volume of sample illuminated, V_0 is the volume of the unit cell, θ is the Bragg angle of the reflection, P is the polarization factor, A is the absorption correction factor and D is the detector efficiency. The additional specific problems of wavelength overlap and normalization could be solved by either an energy-dispersive detector with position sensitivity or a more conventional system consisting of an area detector and a crystal monochromator. In the first case, the full diffraction pattern could be imaged and the intensity of an overlapped spot partitioned among the different reflections producing it. These data could then be used for unit-cell determination, space-group analysis and structure refinement. The ideal detector for this type of system would be a device with the spatial resolution of a CCD or CID and the energy-dispersive resolution of an Si(Li) detector. Both CCDs and CIDs have the potential to work in this manner, the question at present is whether they have high enough speed and radiation stability to be practical. The second type of instrument would reduce the Laue experiment to a sum of many nearly monochromatic data sets. The system would slowly scan through a selected range of energies with a crystal monochromator. At intervals the diffraction pattern would be read and the image saved. The sum of a series of images would be a conventional Laue pattern. This type of imager is clearly feasible and could be readily constructed to test analysis strategies and for comparison with the first instrument. For most other purposes, this system would have no advantages over traditional methods since it eliminates the main advantage of the potential speed inherent in the Laue experiment. The greatly increased amount of data collected in the course of an experiment might also prove cumbersome. Future work will further constrain the factors in equation (3) in systems similar to those described here with a goal of complete structure analysis on a laboratory scale using Laue diffraction.

The authors would like to thank Bob Wentink of CID Technologies for his generous support, Dr Michael Bruck in the Molecular Structure Laboratory for assistance with the use of the CAD-4 diffractometer, Dr Hans Roehrig of the Department of Radiology for his generous loan of the MIN-R medium X-ray phosphor, Michelle Anderson and Dr Neal Armstrong for the gift of the MoS_2, Dr Michael Carducci for the gift of the phosphomolybdenum complex, and Robert Fields for initial investigations of CIDs for direct detection of X-rays. Finally, special thanks are due to Dr John Enemark for suggesting the Laue diffraction application, Dr Pierre Dhez for suggesting the use of CIDs as detectors for X-rays and use of the Cu source, and Dr Philip Coppens for comments on a draft of this work. This research was supported by a monetary grant from Thermo-Jarrell-Ash corporation and material donations from CID Technologies. Some initial work on this project was done as a special class project in chemistry 517 in the Department of Chemistry at the University of Arizona.

References

Acton, L., Morrison, M., Janesick, J. & Elliott, T. (1991). In *Charge-Coupled Devices and Solid State Optical Sensors II*, SPIE/SPSE Electronic Imaging Science and Technology Conference, Vol. 1447-11. Bellingham, Washington: SPIE.

Allinson, N. M. (1989). *Nucl. Instrum. Methods Phys. Res.* A**275**, 587–596.

Allinson, N. M., Allsopp, D. W. E., Quayle, J. A. & Magorrian, B. G. (1991). *Nucl. Instrum. Methods Phys. Res.* A**310**, 267–272.

Arndt, U. W. (1990). *Synchrotron Radiat. News*, **3**(4), 17–22.

Beker, H., Beusch, W., Campbell, M., Catanesi, M. G., Chesi, E., Clemens, J. C., Delpierrre, P., Di Bari, D., Heijne, E. H. M., Jarron, P., Lenti, V., Manzari, V., Marando, M., Navach F., Neyer, C., Pengg, F., Perego, R., Pindo, M., Quercigh, E., Redaelli, N., Sauvage, D., Segeto, G. & Simone, S., (1993). *Nucl. Instrum. Methods Phys. Res.* A**332**, 188–201.

Bilhorn, R. B. & Denton, M. B. (1989). *Appl. Spectrosc.* **43**, 1–11.

Bilhorn, R. B. & Denton, M. B. (1990). *Appl. Spectrosc.* **44**, 1538–1546.

Campbell, J. W. & Hao, Q. (1993). *Acta Cryst.* A**49**, 889–893.

Carducci, M. (1994). Personal communication.

Carr, P. D., Dodd, I. M. & Harding, M. M. (1993). *J. Appl. Cryst.* **26**, 384–387.

Coppens, P. (1992). *Synchrotron Radiation Crystallography*. New York: Academic Press.

Cruickshank, D. W., Helliwell, J. R. & Moffat, K. (1987). *Acta Cryst.* A**43**, 656–674.

Cruickshank, D. W., Helliwell, J. R. & Moffat, K. (1991). *Acta Cryst.* A**47**, 352–373.

Delpierre, P., Beusch, W., Bosiso, L., Boutonnet, C., Campbell, M., Chesi, E., Clemens, J. C., Cohen-Solal, M., Debusschere, I., Diereckx, B., Enz, C., Focardi, E., Forti, F., Glaser, M., Heijne, E., Hermans, L., Hurst, R., Karar, A., Krummenacher, F., Jaegar, J. J., Jarron, P., Lemeilleur, F., Nava, F., Neyer, C., Ottaviani, G., Potheau, R., Quercigh, E., Redaelh, N., Rossi, L., Sauvage, D., Tonelli, G., Vanstraelen, G., Vegni, G., Viertel, G. & Waisbard, J. (1992). *Nucl. Instrum. Methods Phys. Res.* A**315**, 133–138.

Fields, R., Dhez, P., Slaughter, J., Falco, C. & Denton, M. (1992). *Preliminary Results Using a Charge-Injection Device as an Imaging X-ray Detector*. Presented at the 2nd International Conference on Scientific Optical Imaging.

Gomez de Anderez, D., Helliwell, M., Habash, J., Dodson, E. J., Helliwell, J. R., Bailey, P. D. & Gammon, R. E. (1989). *Acta Cryst.* B**45**, 482–488.

Hao, Q., Campbell, J. W., Harding, M. M. & Helliwell, J. R. (1993). *Acta Cryst.* A**49**, 528–531.

Helliwell, J. R. (1992). *Macromolecular Crystallography with Synchrotron Radiation*. Cambridge Univ. Press.

Helliwell, J. R., Habash, J., Cruickshank, D. W. J., Harding, M. M., Greenhough, T. J., Campbell, J. W., Clifton, I. J., Elder, M., Machin, P. A., Papiz, M. Z. & Zurek, S. (1989). *J. Appl. Cryst.* **22**, 483–497.

Helliwell, M., Gomez de Anderez, D., Habash, J., Helliwell, J. R. & Vernon, J. (1989). *Acta Cryst.* B**45**, 591–596.

Herve, D., Lefesvre, I. & Dupont-Nivet, E. (1992). *RADECS91, First European Conference on Radiation and its Effects on Devices and Systems*, pp. 343–347. New York: IEEE.

Janesick, J., Elliott, T., Bredthauer, R., Chandler, C. & Burke, B. (1988). *X-ray Instrumentation in Astronomy II*, SPIE Vol. 982, pp. 70–94. Bellingham, Washington: SPIE.

Janesick, J. R., Klaasen, K. P. & Elliott, T. (1987). *Opt. Eng.* **26**, 972–980.

Li, Y., Phillips, W. C., Stanton, M. & Kalata, K. (1992). *Nucl. Instrum. Methods Phys. Res.* A**322**, 116–125.

Lumb, D. H. (1990). *Nucl. Instrum. Methods Phys. Res.* A**290**, 559–564.

Lumb, D. H. & Nousek, J. A. (1992). *IEEE Trans. Nucl. Sci.* **39**(5), 1379–1383.

Michon, G. & Burke, H. K. (1973). *Digest of Technical Papers IEEE International Solid-State Circuits Conference 1973*, Vol. 16, pp. 138–139. New York: Lewis Winner.

Michon, G. (1987). US Patent No. 4689-688 (25 August 1987).

Miyahara, J., Takahashi, K., Amemiya, Y., Kamiya, N. & Satow, Y. (1986). *Nucl. Instrum. Methods Phys. Res.* A**246**, 572–578.

Mortara, L. & Fowler, A. (1981). *SPIE Proceedings*, Vol. 290, *Solid State Imagers for Astronomy*, pp. 28–33. Bellingham, Washington: SPIE.

Phillips, W. C., Li, Y., Stanton, M., Xie, J. & O'Mara, D. (1993). *Nucl. Instrum. Methods Phys. Res.* A**334**, 621–630.

Pilon, M. J. (1991). PhD dissertation, Univ. of Arizona, USA.

Roy, T., Watts, S. J. & Wright, D. (1989). *Nucl. Instrum. Methods Phys. Res.* A**275**, 545–557.

Sims, G. (1989). PhD dissertation, Univ. of Arizona, USA.

Sims, G. & Denton, M. B. (1987*a*). *Opt. Eng.* **26**(10), 999–1007.

Sims, G. & Denton, M. B. (1987*b*). *Opt. Eng.* **26**(10), 1008–1019.

Sweedler, J., Denton, M. B., Sims, G. & Aikens, R. (1987). *Opt. Eng.* **26**(10), 1020–1028.

True, J. B., Hanley, Q. S., Gilmore D. A. & Denton, M. B. (1994). Unpublished results.

Van Gordon, S. & Carbone, J. (1994). Personal communication.

Van Gordon, S., Hutton, J., Fassett, D. & Carbone, J. (1993). In *Proceedings of SPIE Conference*, Vol. 1900-1915. Bellingham, Washington: SPIE.

Van Gordon, S. & Zarnowski, J. (1995). Personal communication.

Wyckoff, R. W. G. (1963). *Crystal Structures*, 2nd ed., Vol. I, New York: John Wiley.

Xuong, N. H., Freer, S. T., Hamlin, R., Nielson, C. & Vernon, W. (1978). *Acta Cryst.* A**34**, 289–296.

Zarnowski, J., Carbone, J., Carta, R. & Pace, M. (1994). In *Proceedings of SPIE Conference*, Vol. 2172-16. Bellingham, Washington: SPIE.